Available online at www.sciencedirect.com
ScienceDirect
Remote Sensing of Environment 112 (2008) 2711–2726
Remote Sensing of Environment
www.elsevier.com/locate/rse

Validation of GOES and MODIS active fire detection products using ASTER and ETM+ data

Wilfrid Schroeder [a,*], Elaine Prins [b], Louis Giglio [c], Ivan Csiszar [a], Christopher Schmidt [b], Jeffrey Morisette [d], Douglas Morton [a]

[a] Department of Geography University of Maryland College Park, MD 20742, United States
[b] Cooperative Institute for Meteorological Satellite Studies, University of Wisconsin at Madison, WI 53706, United States
[c] Science Systems and Applications Inc., Lanham MD 20706, United States
[d] NASA's Goddard Space Flight Center Code 614.5 Greenbelt, MD 20771, United States

Received 28 August 2007; received in revised form 3 January 2008; accepted 4 January 2008

Abstract

In this study we implemented a comprehensive analysis to validate the MODIS and GOES satellite active fire detection products (MOD14 and WFABBA, respectively) and characterize their major sources of omission and commission errors which have important implications for a large community of fire data users. Our analyses were primarily based on the use of 30 m resolution ASTER and ETM+ imagery as our validation data. We found that at the 50% true positive detection probability mark, WFABBA requires four times more active fire area than is necessary for MOD14 to achieve the same probability of detection, despite the 16× factor separating the nominal spatial resolutions of the two products. Approximately 75% and 95% of all fires sampled were omitted by the MOD14 and WFABBA instantaneous products, respectively; whereas an omission error of 38% was obtained for WFABBA when considering the 30-minute interval of the GOES data. Commission errors for MOD14 and WFABBA were found to be similar and highly dependent on the vegetation conditions of the areas imaged, with the larger commission errors (approximately 35%) estimated over regions of active deforestation. Nonetheless, the vast majority (>80%) of the commission errors were indeed associated with recent burning activity where scars could be visually confirmed in the higher resolution data. Differences in thermal dynamics of vegetated and non-vegetated areas were found to produce a reduction of approximately 50% in the commission errors estimated towards the hours of maximum fire activity (i.e., early-afternoon hours) which coincided with the MODIS/Aqua overpass. Lastly, we demonstrate the potential use of temporal metrics applied to the mid-infrared bands of MODIS and GOES data to reduce the commission errors found with the validation analyses.

Keywords: Vegetation fires; Amazonia; MODIS; GOES; ASTER; ETM+

1. Introduction

Vegetation fires, in combination with deforestation activities, result in the conversion and the alteration of large areas of evergreen tropical forests, transitional forests and savanna vegetation throughout the tropics each year (Cochrane et al., 1999; Nepstad et al., 1999). Brazilian Amazonia currently represents one of the most active regions of deforestation and biomass burning in the world (Csiszar et al., 2005; Dwyer et al., 2000; Giglio et al., 2006). Widespread use of fires for land clearing and management necessitates consistent methods for monitoring and mapping biomass burning on a routine basis (Korontzi et al., 2004; Schroeder et al., 2005). Satellite imaging systems have been providing systematic observations of fire activity over Amazonia for more than two decades (Prins & Menzel, 1994; Setzer & Pereira, 1991). Reliance on remote sensing active fire products is strongly reinforced in the region as a consequence of the inherent difficulty in documenting fire activity through ground observations over an area of 5 million

* Corresponding author. 2181 LeFrak Hall, Department of Geography, University of Maryland, College Park, MD 20742, United States.
E-mail address: schroeder@hermes.geog.umd.edu (W. Schroeder).

0034-4257/$ - see front matter © 2008 Elsevier Inc. All rights reserved.
doi:10.1016/j.rse.2008.01.005

km^2 with limited infrastructure and a sparse road network. Remotely sensed active fire data are now routinely used to feed regional fire alert systems (CONAE, 2007; CPTEC, 2007; DIMARENA, 2007), as well as biomass burning emissions models which are key to helping us understand some of the fundamental issues involving carbon cycle dynamics in Amazonia and its effects on climate and air quality (Freitas et al., 2005; Van der Werf et al., 2003).

The number of operational or near-operational fire products serving Amazonia has increased considerably in the past decade as a result of growing demand for fire information from the regional and global scientific communities, environmental enforcement agencies, and other end users. Information on fire activity for Amazonia is currently available from geostationary and polar orbiting satellites (CPTEC, 2007; Govaerts, et al., 2007; UW Madison CIMSS, 2007). The increased observation frequency provided by geostationary data can be used to help delineate the diurnal cycle of fires, an important measure of fire activity distribution throughout the day (Prins & Menzel, 1992, 1994; Menzel & Prins, 1996). The fire diurnal cycle signature becomes particularly pronounced in tropical areas such as Brazilian Amazonia, where humans play an important role as the ignition source (Giglio, 2007; Kaufman et al., 1998; Prins et al., 1998).

While some studies have assessed the performance of the polar orbiting and geostationary active fire products through validation exercises (Menzel & Prins, 1996; Prins et al., 1998; Morisette et al., 2005a; Morisette et al., 2005b; Csiszar et al., 2006), detailed characterization of these products on a regional to sub-continental scale is still needed. The increased demand for these products requires that an effort be made to fully characterize the quality of their data.

In this study we investigate the performance of two major active fire detection products derived from the polar orbiting Moderate Resolution Imaging Spectroradiometer (MODIS), on board the EOS-AM (Terra) and EOS-PM (Aqua) satellites, and the imager on board the Geostationary Operational Environmental Satellite, positioned at 75°W longitude along the equator (GOES-East). We focus our analyses on Brazilian Amazonia using a large selection of scenes from the Advanced Spaceborne Thermal Emission and Reflection Radiometer (ASTER) and the Landsat 7 Enhanced Thematic Mapper Plus (ETM+) at 30 m resolution to serve as our "ground truth" data to validate the coarser resolution products. The scene selection covers a wide range of vegetation fire conditions that are found across the study region. We rigorously test the accuracy of the MODIS and GOES active fire products to quantify sources of commission and omission errors, and suggest a method to enhance the current contextual fire detection algorithms using brightness temperature profiles to reduce the commission error rate over tropical forest regions. We apply a bottom-up approach by associating the fire statistics derived from the 30 m resolution data to the moderate and coarse resolution data of MODIS and GOES, respectively. Complementary *in-situ* measurements are also used in this study along with data from an airborne imaging instrument to independently analyze the properties of the fires mapped by the orbital systems.

2. Data

The data used in this study cover nine states that form the Legal Brazilian Amazon, an area characterized by a large gradient of percentage tree cover (see Fig. 1). In order to represent all of this variation in the validation process of GOES and MODIS, a large volume of data was processed. The details of each individual data set are given below:

2.1. GOES

The study region is centered within the regular scanning zone of the GOES East imager which produces 4×4 km resolution images at 30 min intervals. Centered in the fire sensitive mid-infrared region of 3.8–4.0 μm, channel 2 provides the primary radiometric measurement for GOES imager fire detection. In order to increase our sample size, we used a combination of versions 5.9 (2000–2002) and 6.0 (2002–2005) of the Wildfire Automated Biomass Burning Algorithm (WFABBA) generated by the Cooperative Institute for Meteorological Satellite Studies (CIMSS) at the University of Wisconsin, Madison. The two products are very similar; changes in version 6.0 were mainly associated with the implementation of more stringent tests to eliminate potential spurious fires from highly reflective clouds (Prins & Menzel, 1994; Prins et al., 2003).

We used the full resolution active fire masks provided by CIMSS as well as the regular ASCII data files commonly available to end users. GOES channel 2 Variable Format (GVAR) data were also obtained from NOAA's Comprehensive Large Array-data Stewardship System (NOAA-CLASS; URL: http://www.class.noaa.gov/saa/products/welcome). The GVAR data were used for the purpose of image registration as well as to derive brightness temperature estimates used in Section 4.4. A total of 119 individual images were used for the validation analysis covering the acquisition dates and hours of ASTER or ETM+ data. An additional 446 images were used in the analyses described in Sections 4.3–4.4.

2.2. MODIS

The two MODIS instruments on board the polar orbiting Terra and Aqua satellites provide daily images of Amazonia at nominal 1×1 km spatial resolution. We used the Collection 4 MODIS Level 2 (unprojected swath) fire product (MOD14) (Giglio et al., 2003), available from NASA's Land Processes Distributed Active Archive Center (LP-DAAC) (URL:http://edcimswww.cr.usgs.gov/pub/imswelcome/), in conjunction with the MODIS geolocation product (MOD03), available from NASA's Level 1 and Atmosphere Archive and Distribution System (URL: http://ladsweb.nascom.nasa.gov/data/). A total of 135 data granules (5-minute orbit segments) from Terra MODIS were used for the validation analyses coinciding with the acquisition dates of our 2001–2005 ASTER scenes. An additional 164 MOD14 data granules were used along with the corresponding Level 1B Calibrated Radiance granules (MOD021km) to support the analyses described in Sections 4.3–4.4.

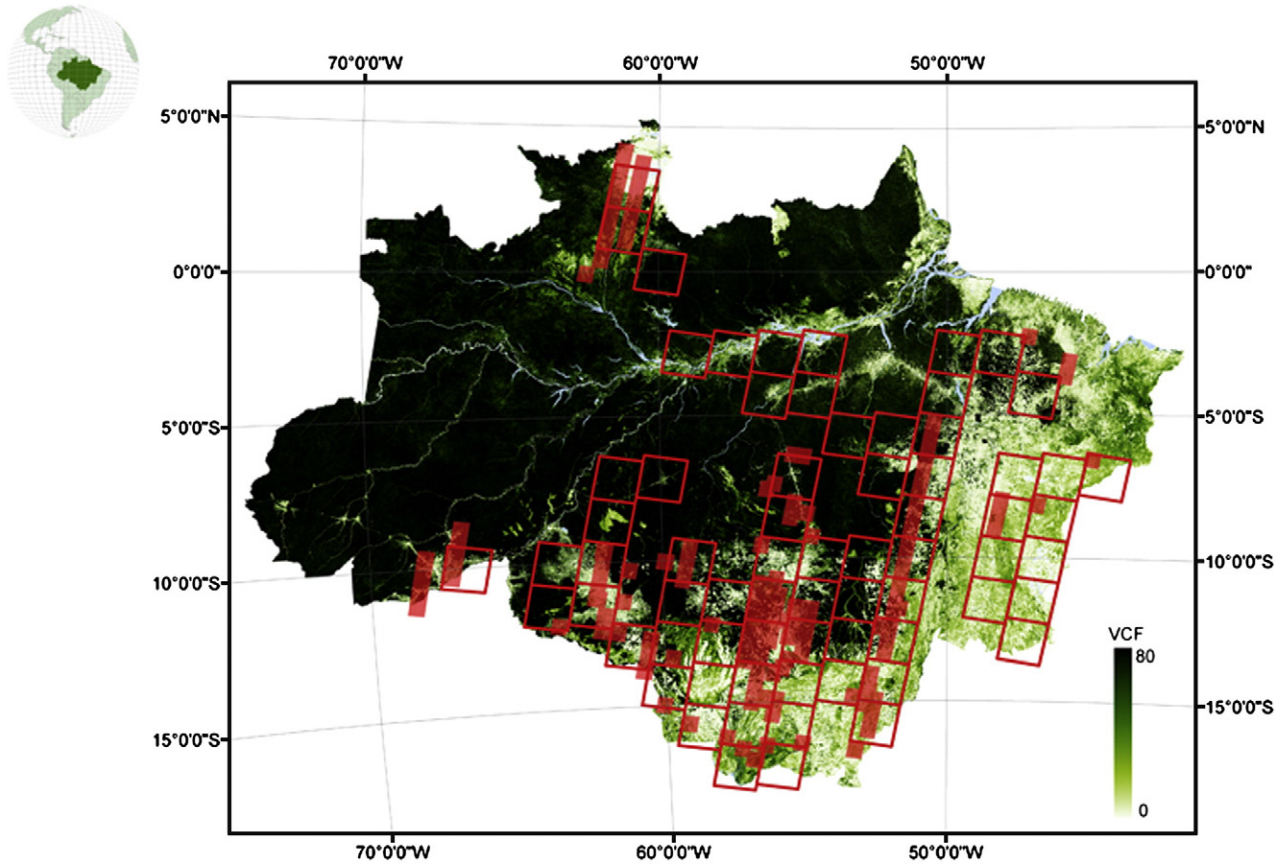

Fig. 1. Location of ASTER (shaded red areas) and ETM+ (red boxes) scenes used to validate the MOD14 and WFABBA fire detection products, over percentage tree cover data (Hansen et al., 2002).

2.3. ASTER

ASTER is an on-demand radiometer flying on board the Terra satellite and therefore it collects data simultaneously with Terra MODIS (Yamaguchi et al., 1998). Although the instrument does not possess a mid-infrared channel, active fire detection was proven successful in previous studies by combining the top of the atmosphere (TOA) reflectance estimates from channel 3 near infrared data resized from 15 to 30 m resolution and channel 8 short wave infrared data at 30 m resolution (Table 1) (Morisette et al., 2005a; Giglio et al., in press). We used a total of 162 ASTER Level 1B "Registered Radiance at the Sensor" scenes obtained from the LP-DAAC (Fig. 1).

2.4. ETM+

The ETM+ instrument flies on board Landsat-7, which has a similar orbital path as the Terra satellite, albeit with an earlier daytime equator crossing time of 1000 (Goward et al., 2001). The spatial and spectral specifications of ETM+ channels 4 and 7 are similar to those of ASTER channels 3 and 8, respectively, making ETM+ equally suitable for active fire mapping (see Appendix A). In this study we used 123 scenes available through the National Institute for Space Research (INPE, Brazil) and the Global Land Cover Facility (GLCF; URL: http://glcf.umiacs.umd.edu/index.shtml). The scenes covered the period from 2000–2003.

2.4.1. Vegetation data

The 500 m percentage tree cover data derived from the MODIS Vegetation Continuous Fields (VCF) (Hansen et al., 2002) Collection 4 product was used in this study to stratify the study region into vegetation sub-groups. A total of 12 MODIS 10°×10° Sinusoidal Projection tiles were required to produce a mosaic covering the entire study region. The annual VCF product for 2000–2005 was available through GLCF.

Table 1
Main characteristics of the satellite imagery used

Instrument	Primary Bands Used for Fire Detection	Spatial Resolution	Temporal Resolution	Number of images
GOES Imager	Channel 2: 3.80–4.00 μm	4 km	30 min	565
MODIS	Channels 21 & 22: 3.929–3.989 μm	1 km	1–2days	299
ASTER	Channel 8: 2.295–2.365 μm	30 m	16days	162
ETM+	Channel 7: 2.09–2.35 μm	30 m	16days	123

2.4.2. Ground data

In-situ fire temperature measurements were obtained for seven different burning locations. These measurements were derived as part of validation campaigns implemented during 2003–2004 when prescribed burns were arranged in different parts of the study region. We used a thermocouple linked to a data logger (Campbell Scientific Inc. CR21X) which recorded the development of the fire fronts at 0.2 Hz for the duration of the burning (i.e., from fire onset through the smoldering phase). These measurements were mainly intended to characterize the differences in fire intensity and duration among the main fire types typically observed in the study region.

2.4.3. Airborne data

Airborne data were acquired for Roraima state in northern Brazilian Amazonia using the Airborne Hyperspectral Scanner (AHS AA5201, Argon ST) over two prescribed burns and over 90 randomly chosen fires during a 7-day field campaign in January 2003. The AHS sensor consists of a 50 channel scanner covering 0.445–12.08 μm. The instrument is owned and operated by the System for the Protection of Amazonia (SIPAM) and it was first flown over vegetation fires during the field campaign in January 2003. We applied supervised tests to the data in order to produce fire masks at ground resolutions of 1–1.65 m. The fire masks were used to delineate the contour of the active flaming areas in each image.

3. Methods

Three previous studies relied on ASTER data to validate the Terra MODIS active fire detection product. First, Morisette et al. (2005a) used 18 ASTER scenes from August–October 2001 to validate the MOD14 collection 3 and 4 products over Southern Africa. Next, Morisette et al. (2005b) used 22 ASTER scenes to simultaneously validate two different active fire detection products based on Terra MODIS data for three sites in Brazilian Amazonia. Lastly, Csiszar et al. (2006) used 131 ASTER scenes to validate the MOD14 collection 4 product over Siberia. All three studies used active fire masks derived from ASTER imagery to validate the coincident Terra MODIS active fire product.

In order to validate and characterize the MOD14 fire product over Brazilian Amazonia, we used a similar approach as described in the studies listed above. We produced active fire masks for all 162 ASTER scenes using a contextual approach based on ASTER channels 3 (0.76–0.86 μm) and 8 (2.295–2.365 μm) (Giglio et al., in press). The resulting 30-m mask indicates the presence ("1") or absence ("0") of active fires within each pixel, and pixel counts are used as surrogates for actively burning area. We recognize this is still an intermediate step towards deriving validation statistics based purely on "true" physical quantities defining fires.

We used information from the Terra MODIS geolocation product (MOD03) to overlay the MOD14 product on top of the ASTER fire masks. From the fire mask data we derived the sum of 30-m active fire pixels and the number of individual fire clusters within each MODIS pixel. These statistics were used to determine the detection performance of the MODIS instrument by means of a statistical logistic regression model defined as:

$$P(x_i) = \frac{e^{\alpha + \sum_{j=1}^{n} \beta_j x_{ij}}}{1 + e^{\alpha + \sum_{j=1}^{n} \beta_j x_{ij}}}. \quad (1)$$

Here $P(x_i)$ is the probability of detection (0–1) of MODIS pixel i based on the linear combination of ASTER fire pixel summary statistics ($j=1,n$), and α and β_j are parameters derived from the data (Agresti, 1990; Morisette et al., 2005b). Error matrix analysis was also applied using information on the number of 30-m active fire pixels to produce empirical curves defining the omission error estimates for the MODIS fire product.

In order to account for the effects of the MODIS triangular point spread function (Wolfe et al., 2002), the projected surface area for the MODIS pixel was considered equal to 2×1 km at the sub-satellite point. This procedure is applied for all MODIS pixels overlapping the ASTER image.

We tested the consistency of the fire masks using 1.5 m resolution data from the AHS instrument over two prescribed burns conducted in January 2003 which were coincident with ASTER imaging (Fig. 2). Additionally, hundreds of image quick looks were produced to verify the consistency of the MOD14 detections when overlaid on top of the ASTER fire masks and false color composites.

Our validation analyses of the GOES active fire detection product followed a similar approach to the one described above for the MODIS data. However, three major issues necessitated that a slightly different processing scheme be used for the GOES data:

(i) Temporal differences in image acquisition needed to be considered in order to avoid the effects of short-term changes in fire characteristics. As part of our field campaign in January 2003, multi-temporal data from the AHS instrument were acquired during a prescribed burn of a 75 ha deforestation plot in Roraima state. Approximately 1.5 h of fire activity was monitored by the AHS instrument at 1.5 m resolution. Once the fire lines were well established and moving freely, four sequential AHS images were produced separated by 5-minute intervals from each other. We found the instantaneous fire-affected areas to be within 10% of the mean estimated area (35 ha) mapped during the 20-minute interval. In a separate study, Csiszar and Schroeder (2007) used ETM+ and ASTER images acquired 30 min apart to assess the impact of varying fire conditions on the performance of the MODIS active fire product. Their results suggested that short-term changes in vegetation fire conditions have only a minor impact on moderate resolution active fire products. In this study we adopted a conservative approach limiting the use of the 119 GOES images selected for the validation analysis to within 15 min of the acquisition of the available higher resolution data.

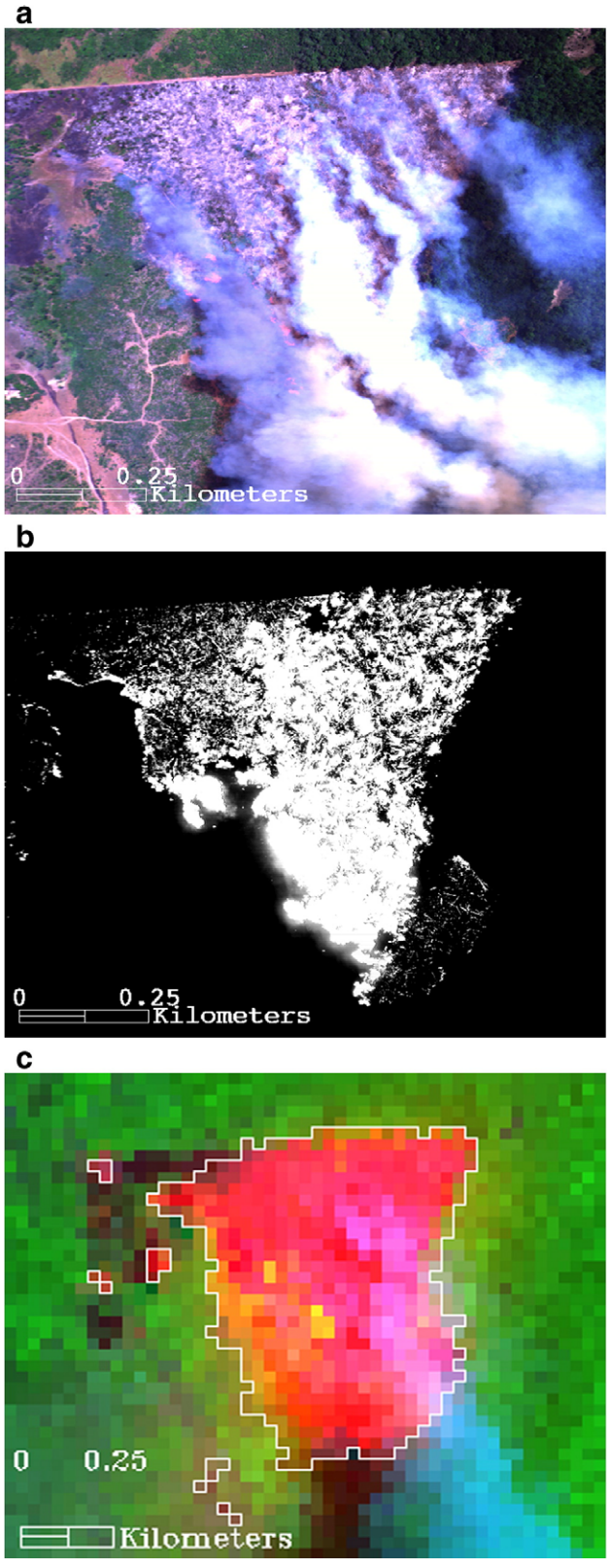

Fig. 2. Prescribed burn of a deforestation plot located at 1°35'08" N 60°57'18"W on January 28, 2003. (a) 1.5 m resolution data from AHS RGB combination of bands 9 (0.685 μm), 5 (0.565 μm) and 1(0.445 μm) acquired at 1438 UTC; (b) fire mask derived from AHS band 43 (4.95 μm); (c) ASTER image of the same fire (RGB bands 8-3-1) acquired at 1436 UTC. The fire perimeter (white contour) derived from the ASTER fire mask is also shown in (c).

(ii) Navigation errors are known to affect the GOES images on a regular basis, and image geolocation problems can occur even between 30-minute acquisitions (Menzel & Purdom, 1994). To eliminate the problem, all GOES images used were manually co-registered to within 1 pixel.

(iii) Due to the coarse resolution of the GOES imager, fewer pixels are sampled compared to MODIS for the same area covered by ASTER. Consequently, a larger number of ASTER scenes must be processed in order to create an equivalent sample size. Alternatively, one can use ETM+ data to increase the area covered by each scene processed (see Appendix A). Therefore our validation of the WFABBA product used ASTER and ETM+ fire mask data to produce 30 m active fire summary statistics for all co-located GOES pixels within a 15 min window between acquisition times.

For projecting the GOES pixel area on top of the higher resolution data we used a full nominal resolution pixel size in the along and across scan directions (i.e., 4×4 km in size near nadir). We considered this area estimate to be a good balance between the pixel size resulting from the over-sampled image matrix and the pixel dimensions if accounting for the GOES point spread function.

4. Results and discussion

Two major types of fires are normally observed across our study region, namely conversion and maintenance fires. Conversion fires will normally be associated with deforestation activities occurring along the new frontiers of land development dominated by high percentage tree cover (i.e., >60%). As they burn large biomass volumes, these fires will normally be characterized by high flame temperatures followed by a relatively hot smoldering stage which can last from a few hours to a few days (Fig. 3). Maintenance fires are normally used to rejuvenate pastures or to clear crop residue and are particularly important in areas dominated by low percentage tree cover (i.e., <20%). As such, these fires are characterized by relatively low flame temperatures followed by a shorter smoldering stage ranging from a few minutes to a few hours. Compared to conversion fires, maintenance fires show a narrower flaming front as well as a shorter smoldering stage (Fig. 3). Between these two major classes we can also find intermediate fire types (e.g., fires resulting from the clearing of secondary forests and woody *Cerrado* (savannas)) with reduced biomass load compared to old growth or pristine tropical forests. These fires can be more variable in terms of their flame temperature and burning duration (Fig. 3). Data in Fig. 3 suggest that the intensity and duration of conversion fires may facilitate their detection as compared to other types of tropical vegetations fires.

4.1. Overall detection performance

The processing of all pairs of MODIS-ASTER images resulted in approximately 7300 MODIS pixels containing at least one ASTER 30 m active fire pixel. A total of 1640 MOD14 pixels

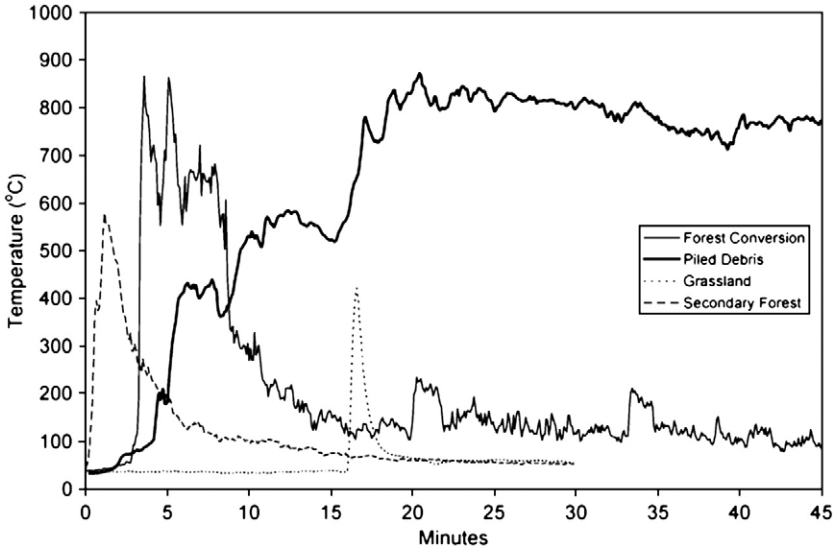

Fig. 3. (a) Typical temperature profiles associated with fires used for: forest conversion, burning of piled debris from deforestation, rejuvenating grassland, and clearing of secondary forest re-growth.

were flagged as "fire" for that data set. The pairs of GOES-ASTER images resulted in approximately 2900 GOES pixels containing at least one ASTER active fire pixel; the pairs of GOES-ETM+ images covered another 14,500 GOES pixels with at least one ETM+ 30 m active fire pixel. This entire dataset included a total of 560 WFABBA fire detections.

Summary statistics were produced from the higher resolution fire masks for all MODIS and GOES pixels sampled. These statistics were used to fit the logistic regression model in Eq. (1), from which the general detection probability curves for MOD14 and WFABBA were derived. The differences in detection performance between the MOD14 and WFABBA fire products are shown in Fig. 4a and b, respectively. However, the distances that separate the curves and the associated performance of the two products are smaller than expected. For the MODIS-ASTER configuration used in this study, all MODIS pixels sampled were imaged close to nadir resulting in pixels with 1 × 1 km nominal spatial resolution. The pairs of GOES-ASTER and GOES-ETM+ images used were acquired under slightly variable conditions in terms of the pixel size sampled, ranging from near nadir geometry to cases where the additional pixel area enlargement was equivalent to about 20%. Consequently, the spatial resolution ratio of MODIS to GOES was always greater than or equal to 16×, which should result in an equivalent difference between their detection performances. However, an approximate ratio equal to or less than 4× separates the pairs of detection curves for each tree-cover interval described by the MOD14 and WFABBA products in Fig. 4a and b.

In the case of Fig. 4, a one-to-one comparison of the two instruments is difficult even for a small case study analysis as differences between products will likely be a result of: (i) varying sensor-target-sun relative positions; (ii) atmospheric attenuation, including fire obscuration by heavy smoke released during burning; (iii) relative position of the actual pixel area in relation to the location of the active fire zone and the effects of the point spread function, (iv) timing of acquisition, etc. Since the actual high-resolution validation datasets for MODIS and GOES are different, some difference in fire types may add uncertainty despite the rigorous sample used for this analysis.

Our field data indicated that conversion and maintenance fires can show temperature variations on the order of hundreds of degrees Kelvins even over very small areas. Consequently, their peak in emittance is likely to spread over a broader spectral interval than most land surfaces (e.g., bare soils and vegetated areas). With the GOES imager having a broader mid-infrared channel compared to MODIS (Table 1), it is plausible that the former will sense the radiative signal from a wider range of fire temperatures. This increase in the fire signal compared to the background could produce a higher relative capacity of GOES to detect them.

4.2. Omission errors

Omission estimates were empirically derived for WFABBA and MOD14 by assessing the number of 30 m active fire pixels corresponding to true fire detections using an error matrix analysis. We counted the number of WFABBA or MOD14 detections for each subset of GOES and MODIS pixels, respectively, showing a number of ASTER or ETM+ fire pixels greater or equal to N. By varying N between 1 and the maximum value in our data set (~1200), we produced the omission error estimates for the two products (Fig. 5).

Two areas of relatively high omission error are found for WFABBA at high counts of 30-m active fire pixels, one around 770 counts and a second one near 350 counts. Visual inspection of the areas affected by such large fires indicated that the vast majority of the events were indeed associated with long fire lines occurring over areas of savanna-like vegetation with associated percentage tree cover typically less than 20%. In this case, the fire characteristics are analogous to the maintenance fire depicted in Fig. 3. Consequently, the total radiant energy released is small compared to other types of fires rendering the detection of such

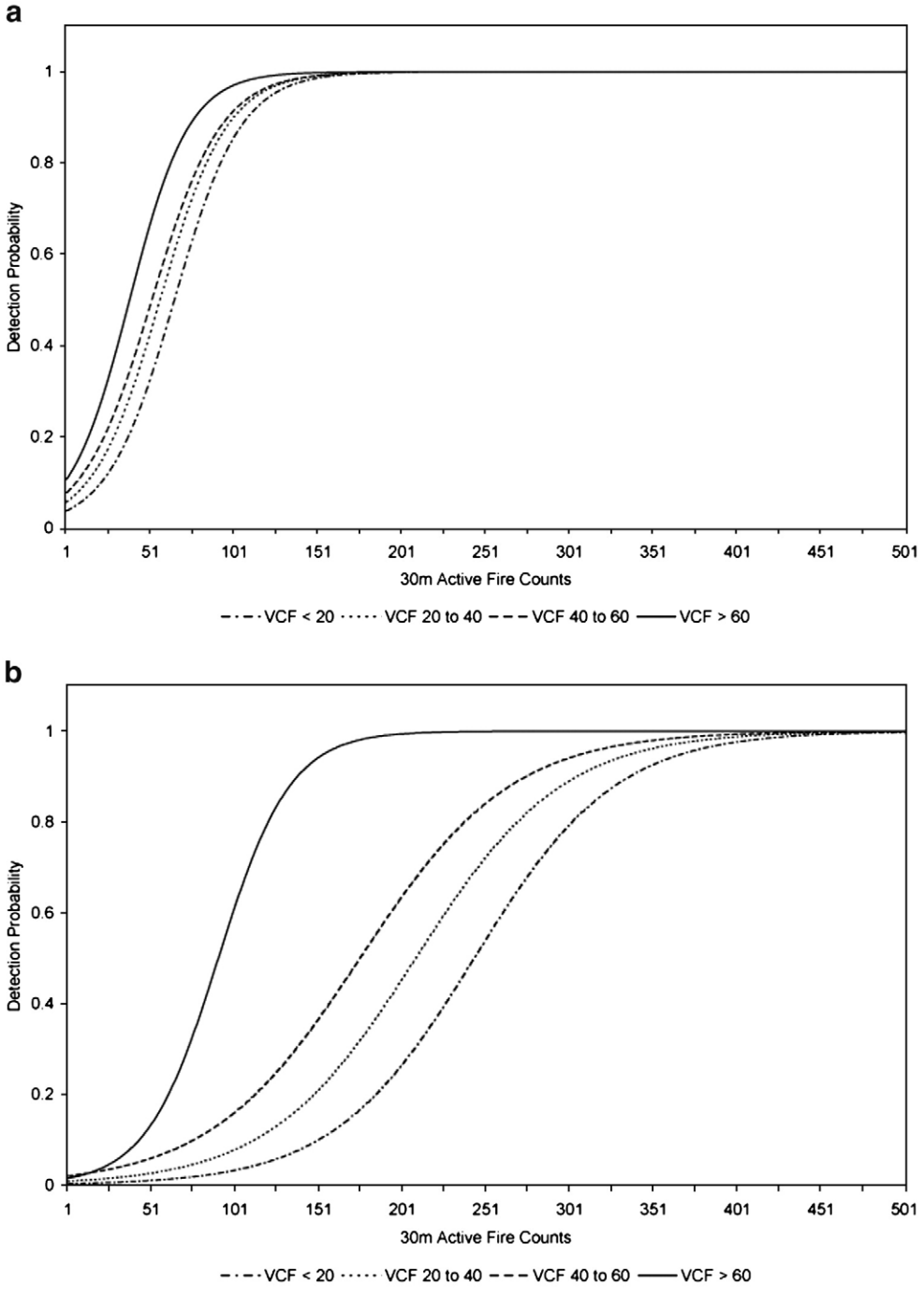

Fig. 4. Fire detection probability curves for MOD14 (a) and WFABBA (b) fire detection products derived for four percentage tree cover intervals.

events less likely. In addition, low thermal contrast with the warmer background was also found to contribute to the reduction in detection performance of WFABBA. In fact, we can distinguish two areas in the MOD14 curve where comparable high count omission errors are found, one near 170 counts and the second one near 245. As with WFABBA, the areas of high count omission in the MOD14 data were also found to be associated with fires occurring at low percentage tree cover areas.

Another factor potentially leading to high count omission errors in the GOES data is related to a nuance of the WFABBA detection algorithm. The detection code includes a persistence check analysis, which takes advantage of the high observation frequency of the GOES imager. The test checks each candidate fire pixel for the presence of any coincident detection in the previous 12 h, allowing some tolerance in the spatial search criterion for small navigation drifts. In doing so, potential spurious detections can be filtered out of the product, therefore reducing commission errors. However, some new or short lived fires may also be removed from the final product. In order to quantify the effects of the temporal filtering, we also plotted in Fig. 5 the corresponding omission error curve derived from the GOES data prior to the application of the persistency test. The

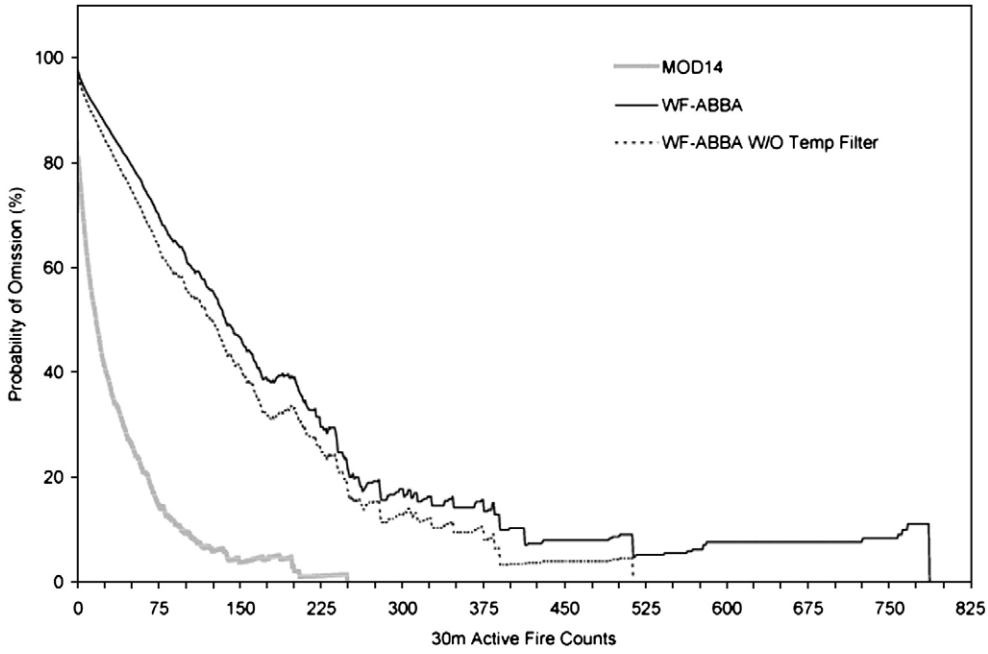

Fig. 5. Omission error estimates produced for MODIS and GOES based on fires sampled at approximately 1030 local time.

result shows a significant increase in the total number of true detections produced (from 458 to 600) and a reduction of the omission errors especially towards the very high counts on the graph.

Although useful for eliminating spurious fires, the application of temporal filters could represent a problem if one considers the instantaneous impact on the omission of relatively large fires that were mistakenly discarded from the final product. However, if such fires persist and maintain or increase their size and intensity in the subsequent GOES observations hours, a second detection will likely occur over time, causing the pixel to pass the persistency test as the previous observations would serve to confirm it. As suggested by previous studies (Giglio 2007; Menzel & Prins, 1996; Prins & Menzel, 1992, 1994; Prins et al., 1998), a strong fire diurnal cycle exists for regions such as Brazilian Amazonia. Under this circumstance, it is expected that fires observed during the mid to late-morning hours imaged by the ASTER and ETM+ instruments will likely grow in size and intensity towards the high peak of fire activity located in the early to mid-afternoon hours. To assess the potential effects of changing fires conditions, we derived the overall omission error estimate for the WFABBA product data using all GOES acquisition hours following the time of observation of the fire event by the higher resolution imagery until about 20:00 h local time. The resulting omission error of 38% indicates that a large fraction of the fires observed in the morning hours which have persisted over subsequent observation hours might have intensified or increased their areas therefore entering the detection envelope of the GOES imager WFABBA fire product.

4.3. Commission errors

False detections were characterized in our analysis as those showing zero 30 m active fire pixels within their footprints. We identified a total of 245 false detections among the 1640 detections produced by the MOD14 product, whereas 102 false detections were identified for WFABBA based on a total of 560 detections sampled by that product. Contrasting surface temperature between the target pixel and its background dominated the false detection occurrences of MOD14 and WFABBA representing 99% and 100% of the cases, respectively. Detection errors caused by the presence of clouds, sun glint zones or anthropogenic sources could not be identified in the data set.

The areas of high thermal contrast were particularly pronounced along the deforestation expansion regions throughout Brazilian Amazonia where relatively cool evergreen tropical forests are replaced by bare soil and senescent grasses — surfaces with increased surface temperature. Despite the differences in instrument characteristics, spatial resolution and algorithm used, both products agree to a large extent in the commission errors produced for all four percentage tree cover intervals considered (Fig. 6). Errors increase rapidly as a function of the percentage tree cover indicating a potentially larger thermal contrast between the target pixel – often characterized by little or no vegetation – and the gradually greener and cooler background.

Detailed inspection of each individual false detection occurrence using all available bands of ASTER and ETM+ at their highest spatial resolution enabled us to refine the classification of those areas and separate them into four different classes (Table 2). The data indicated that a large fraction of the false detections were indeed associated with recent burning activity as confirmed by the presence of fairly homogeneous areas of dark char covering part or all of the MODIS and GOES pixel footprints. Areas of smoldering were also confirmed over a smaller number of cases via the identification of smoke traces or the indication of warm pixels in the short wave infrared channels 8 and 7 of ASTER and ETM+, respectively. When summed, these false detections over areas of fire-related activity corresponded

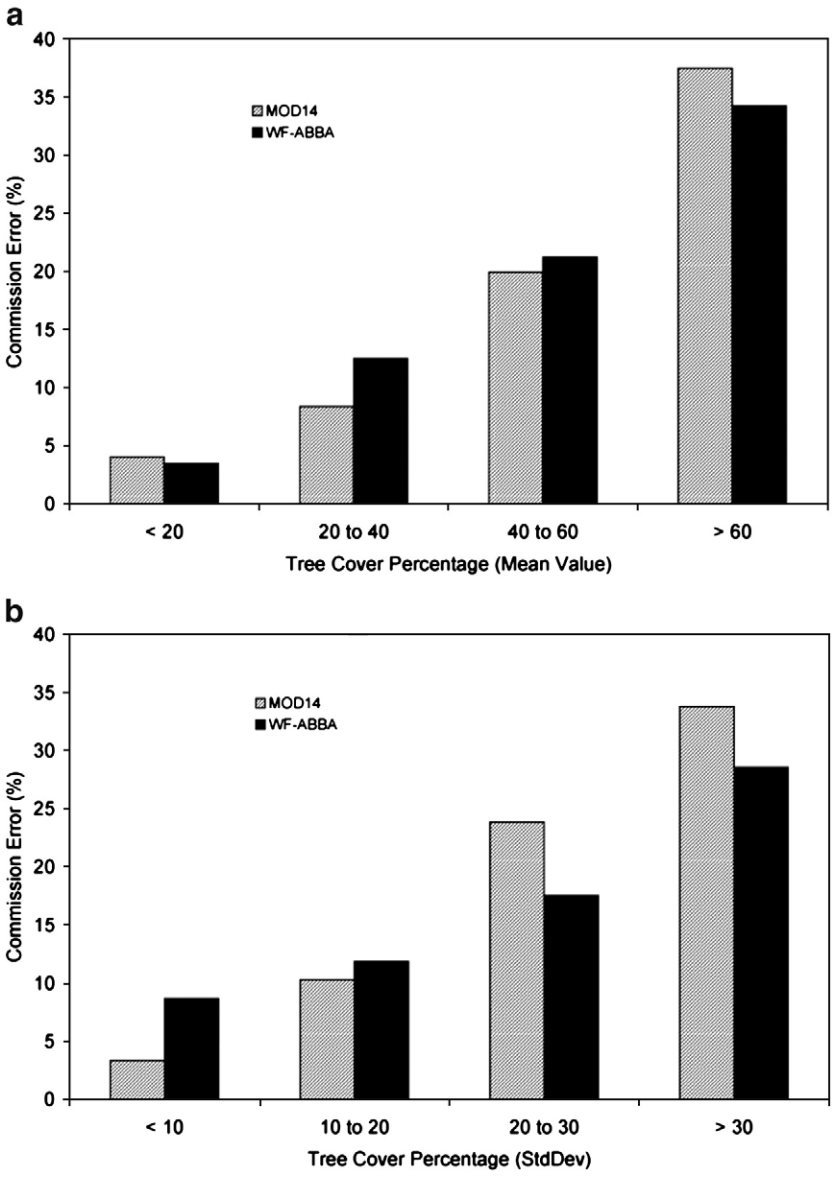

Fig. 6. Commission error estimates for MOD14 and WFABBA. Mean tree cover values (a) estimated for an area of approximately 20×20 km centered on the commission error pixel; standard deviation values (b) determined by sampling a 9×9 pixels window centered on the commission error pixel.

to approximately 87% and 81% of the commission errors of MOD14 and WFABBA, respectively. The remaining false detections were unrelated to fire and mainly the result of warm and reflective bare soils surrounded by contrasting green vegetation. These false detections corresponded to approximately 3% of all detections made by the MOD14 and the WFABBA products. This later result agrees with the findings of Csiszar et al. (2006) for the MOD14 product over Northern Eurasia.

As most of the false detections were associated with areas of recent burning, it is possible that these locations show a strong contrast with their backgrounds for as long as the dark char and ashes remain evenly spread across the burning site. This could lead to repeated false detections affecting those locations over multiple days or even weeks or until the signs of burning are removed from the surface. To investigate this possibility, we checked every false detection location sampled by our data set for the presence of equivalent detections in the previous days. We restricted our analysis to the 30 day period occurring before the observation of the false detection based on the 30 m resolution imagery. The use of a 30 day sampling period was based on the assumption that char and ashes can be removed by wind and rain or by land use (e.g., plowing, seeding, and irrigation). Using spatially coincident 30 m resolution data acquired 16, 32 and 48 days apart we could confirm that scars remained visible for as long as 32 days. For periods greater than that, the burning imprint on the landscape becomes less evident.

Table 2
Classification of MOD14 and WFABBA commission errors based on visual inspection of 30 m RGB composites of ASTER and ETM+ data

Product	Recent Burning (scars visible)	Bare Soil	Smoldering	Spurious detection
MOD14	79%	12%	8%	1%
WFABBA	75%	19%	6%	–

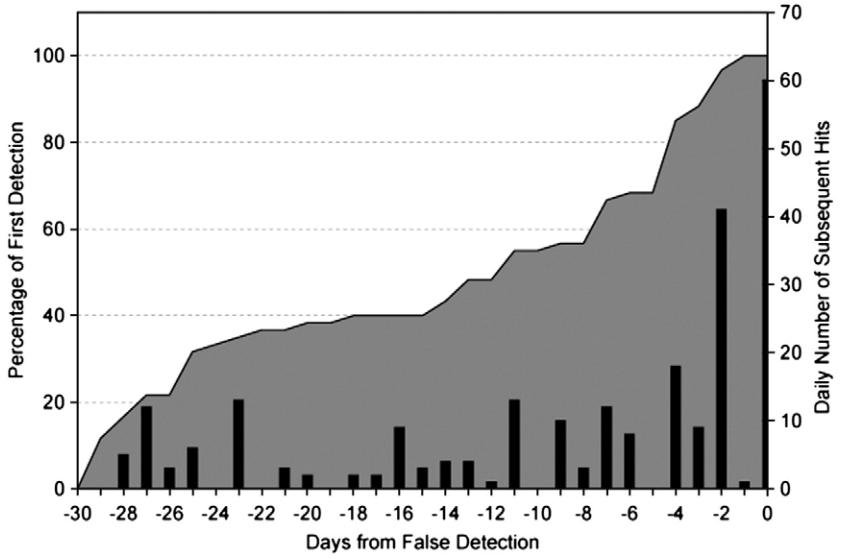

Fig. 7. Daily number of hot spot detections from Terra MODIS (MOD14) and Aqua MODIS (MYD14) data coincident with 60 different locations where MOD14 false detections were identified via 30 m ASTER imagery. The shaded area describes the accumulated percentage of all 60 locations for which a first detection was assigned during the 30-day period before the confirmed false detection.

We searched for all fire detections from Terra (MOD14) and Aqua (MYD14) data co-located to within 1 km of the original false detection. Aqua data was used to improve observation frequency to identify the very first detection made in the 30 day period along with all subsequent ones. Lacking other forms of confirmation, we assigned the actual fire occurrence date to the first detection found for each location and labeled all subsequent detections as potential false detections (Fig. 7). Approximately 60% of the false detections in our data set had co-located detections from MOD14 or MYD14 occurring in the previous 30 days. Of those, about 50% had the first detection occurring in the previous 14 days. The average number of subsequent false detections was 4.

The locations mapped with the analysis above showed that the Terra (MOD14) product produced almost twice as many false detections as Aqua (MYD14) (117 vs. 67). The two products are processed using identical routines, reducing or even eliminating the chance of algorithm artifacts affecting our results. To compare these MODIS results to the GOES data, we analyzed all WFABBA false detections found in our validation data set by monitoring their progress throughout the day. We searched for co-located WFABBA detections occurring during

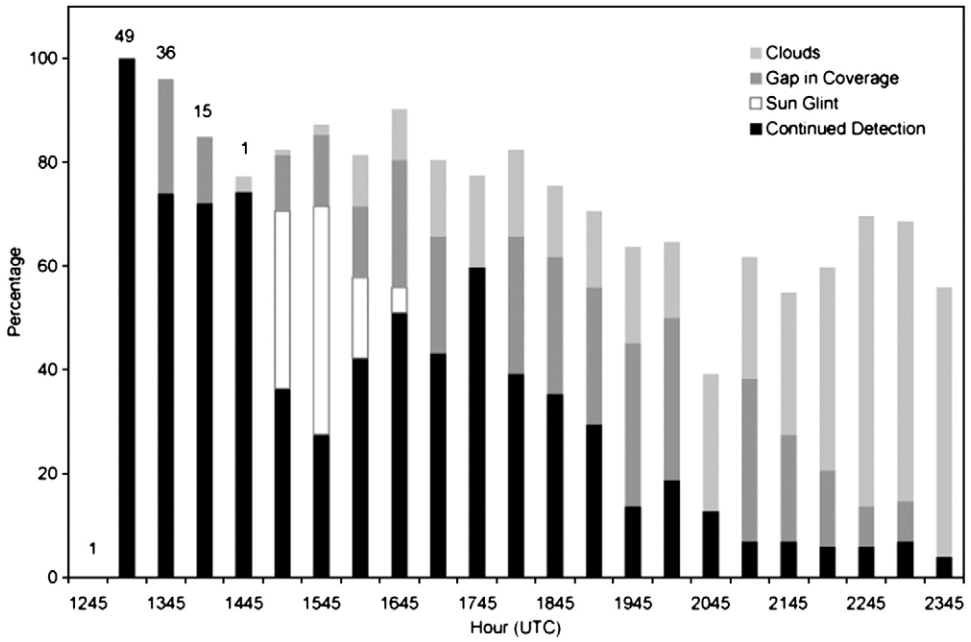

Fig. 8. Half-hourly distribution of WFABBA false detections identified in the validation data set. The absolute number of confirmed false detections identified via ASTER or ETM+ is shown on top of the vertical bars.

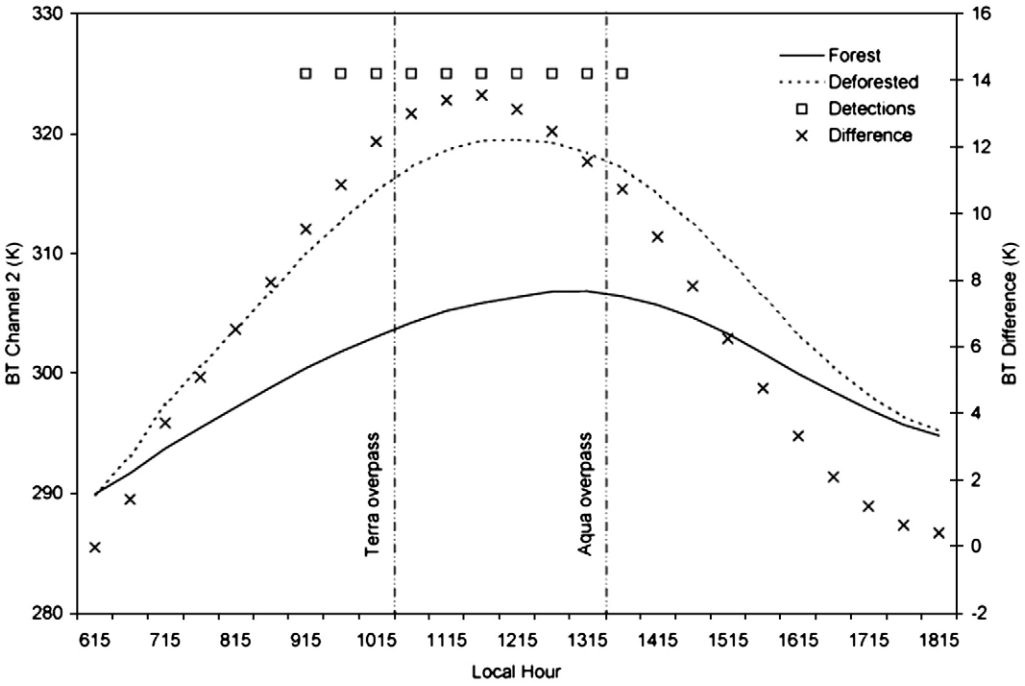

Fig. 9. Diurnal cycle of brightness temperature derived from channel 2 of the GOES imager for two adjacent areas characterized by contrasting vegetation cover conditions. The images were acquired on 04 August 2002 and the forested and deforested areas were located at 11°59'29" 52°49'52"W and 12°06'20 S 52°49'09"W, respectively. The two curves describe the mean values based on 3 and 4 pixels representing the deforested and forest areas, respectively. The occurrence of WFABBA false detections are presented along with the difference between the two curves.

the GOES observation hours made after the false detection was observed. In this case, we applied a search radius of 0.1° (or the equivalent to about 10 km) to allow some flexibility due to potential navigation drift affecting some of the unregistered data used. The number of persisting detections was mapped along with the occurrence of clouds, sun glint areas and gaps in image coverage due to rapid scan operations which could prevent proper observation of the target pixel. The number of false detections persisting in the data gradually decreased with the hours of the day (Fig. 8). At about the same overpass time as Aqua (i.e., 1715–1845 UTC) the number of false detections was reduced by approximately 50%. Our results for the commission errors of GOES (WFABBA) were similar to the results produced for MODIS (MOD14 and MYD14) suggesting a good agreement

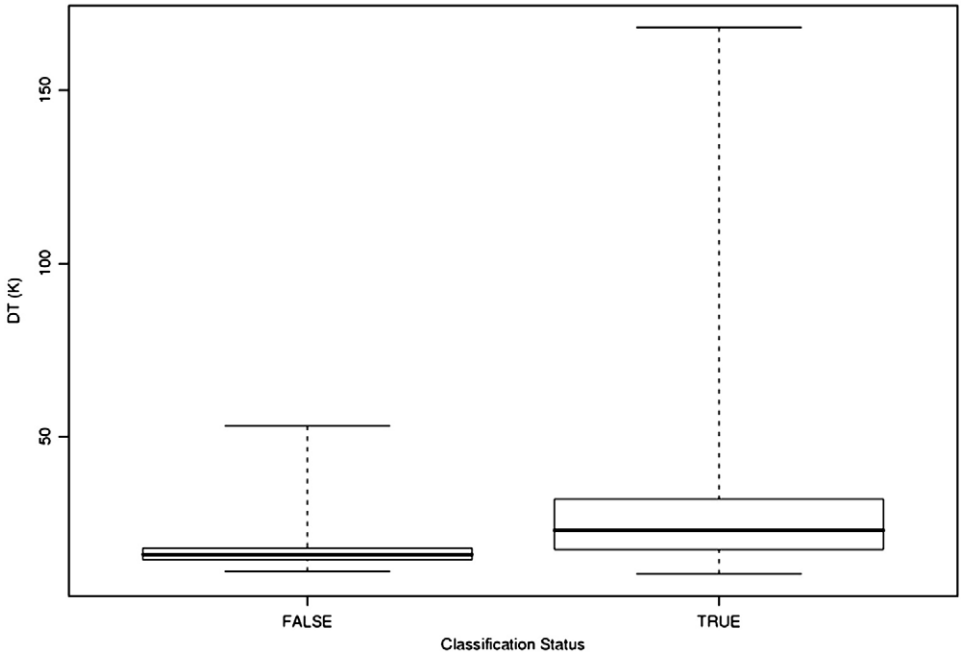

Fig. 10. Boxplots for channel 21 brightness temperature differences between the target pixel and its background for true and false MOD14 detections. Parameters depicted in the plot include: minimum, 25th percentile (lower quartile), mean, 75th percentile (upper quartile) and maximum value.

between the two fire products. Although the WFABBA detection algorithm includes an adjustment to one of the primary tests used (i.e., the brightness temperature (BT) test on channel 2) based on the solar zenith angle measured for every pixel and observation hour ($BT_2 > cosine$ (solar zenith angle)$\times 15$ K$+285$ K), the resulting correction factors for the approximate overpass times of Terra and Aqua were found to be similar for the study region therefore reducing their influence on the result above.

Two major factors can contribute to the reduction in commission errors towards the afternoon hours. First, cloud coverage in tropical areas such as Amazonia may have a pronounced effect limiting the imaging of the land surface by passive remote sensing instruments. The impact of cloud obscuration on the detection of active fires in Amazonia has already been documented and it is suggested to account for an omission rate of approximately 11% of all fires imaged by coarse resolution sensors (Schroeder et al., 2008). In the case of the commission errors reported above however, areas of cloud shadow and semitransparent clouds which may not interfere on the detection of active fires will affect the thermal properties of the surface thereby potentially enhancing their impact beyond the 11% estimate produced for the active fire data.

Changes in the thermal contrast between adjacent areas with different vegetation cover conditions could also influence the commission errors. To test this assumption, we randomly selected 20 areas of low vegetation cover surrounded by forests to evaluate the changes in thermal contrast measured between the two surfaces throughout the day. We used two sets of GOES imagery acquired on 19 September 2001 and 4 August 2002 covering the entire day at 30 min observation frequency. The

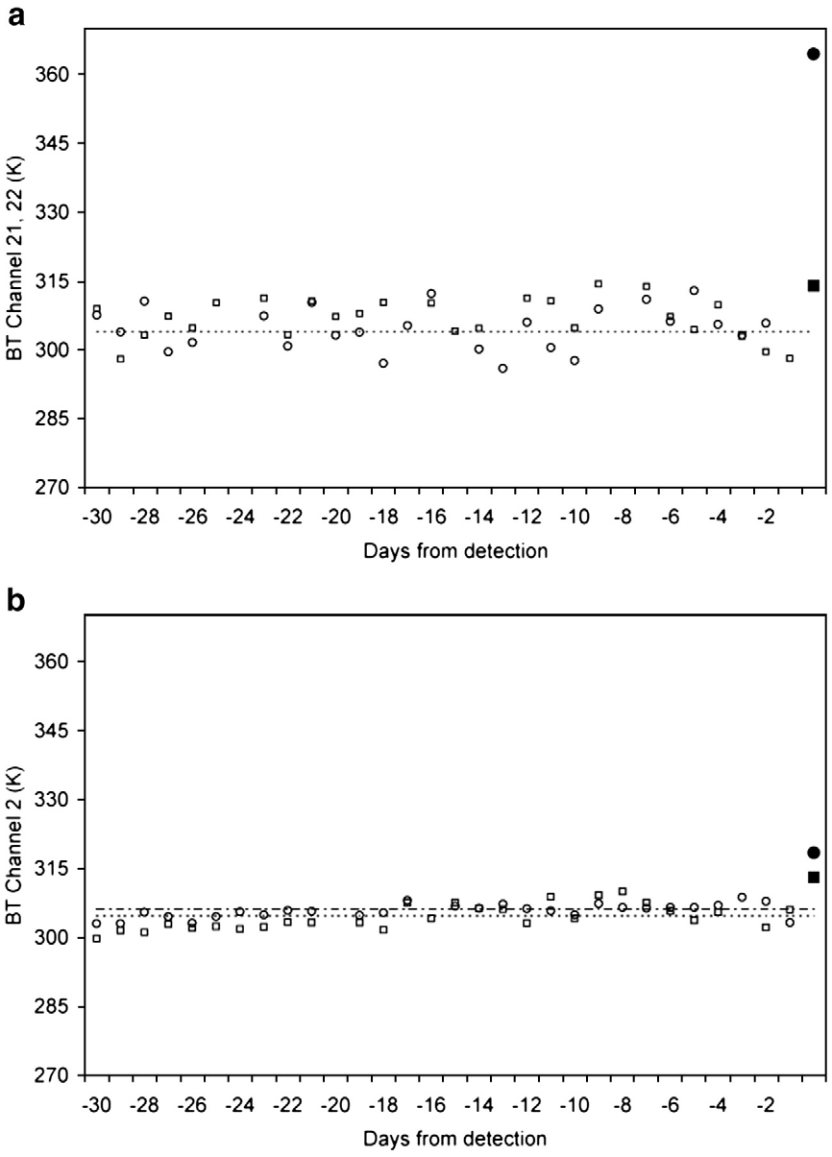

Fig. 11. Brightness temperature (BT) profiles for true (filled circle) and false (filled square) detections using MODIS (a) and GOES (b) data. Open circles and squares represent the BT values during detection-free days. Detection information for the pixels marked in (c–f): false MOD14 detection (c): 55.1237° W 12.129° S, 23 May 2002 at 1403 UTC; true MOD14 detection (d): 56.4828° W 13.225° S, 05 October 2002 at 1409 UTC; false WFABBA detection (e): 50.879° W 8.4169° S, 29 August 2002 at 1315 UTC; true WFABBA detection (f): 50.711° W 10.0335° S, 29 August 2002 at 1315 UTC. False color composites used: 30 m ASTER image (c–d); 30 m ETM+ image (e–f).

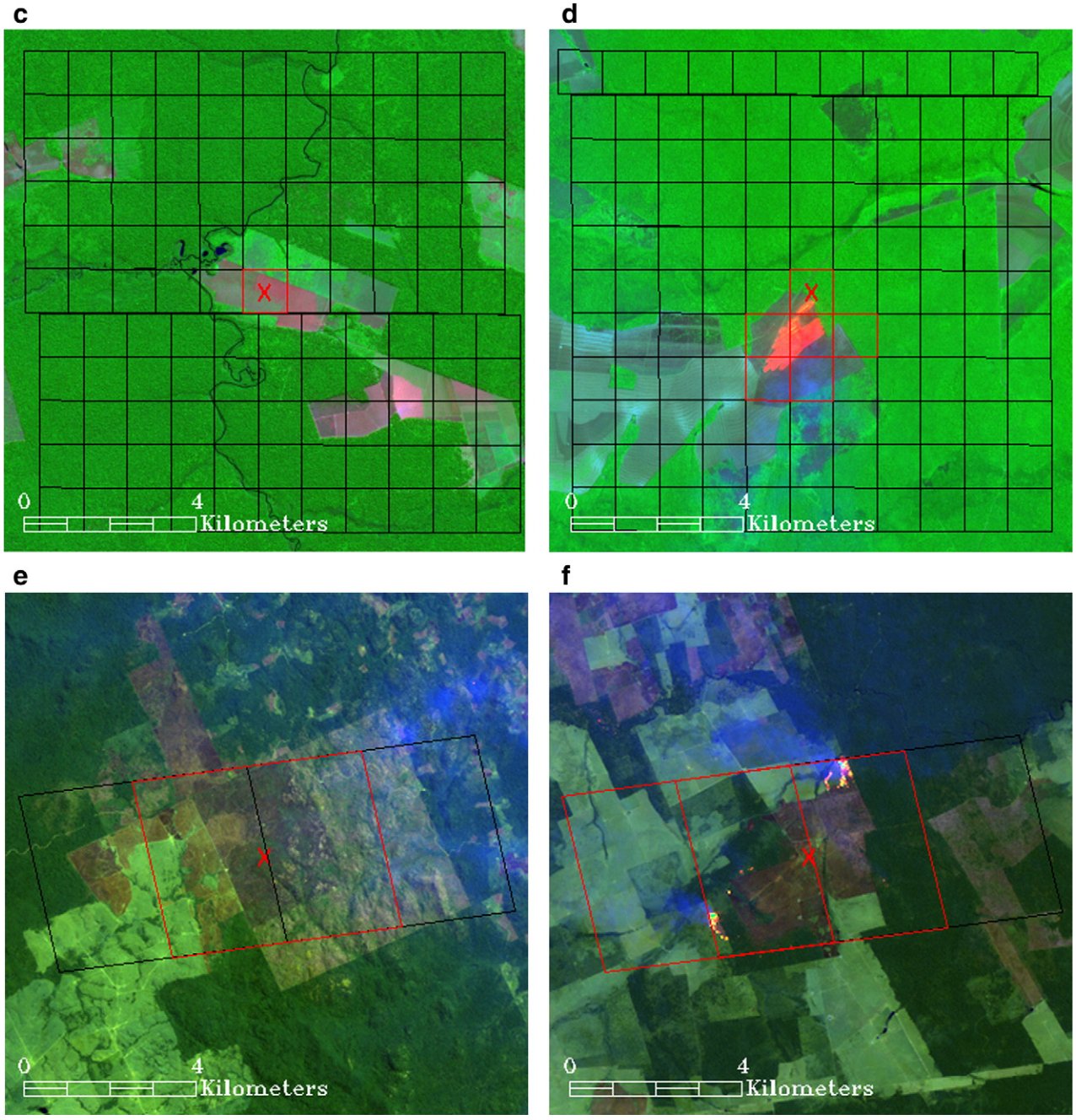

Fig. 11 (*continued*).

two sets of images were characterized by low cloud coverage over the areas of major deforestation activity in Brazilian Amazonia favoring the extraction of cloud free brightness temperature profiles for the selected areas.

Overall, the results showed a decrease in the thermal contrast between forested and non-forested areas measured for the approximate overpass time of Aqua compared to Terra, with the thermal contrast for the latter being 1 K to 10 K greater than the former. Fig. 9 shows the profiles obtained for two adjacent areas of forest and non-forest surfaces where false detections were produced by the WFABBA product. The difference between the two curves is included along with the approximate overpass times for Terra and Aqua. For the particular location used in Fig. 9, clear sky conditions prevailed during the majority of the time. We can see in Fig. 9 that the increased thermal inertia of the forest causes the peak in contrast with the deforested area to move closer to the observation hour of the Terra satellite. The false detections are found equally distributed around the area of greater thermal contrast and therefore tend to become more evident near the observation hours close to the Terra overpass and less so near the observation hour of Aqua. In this case, the reduction in thermal contrast for the two surfaces between the Terra and Aqua overpasses was small (~2 K) and false detections could also be observed until about 15 min after the Aqua overpass time. In other situations where the change in surface conditions between Terra and Aqua overpasses is greater, the

peak in thermal contrast approaches the Terra overpass time leading to fewer false detects during the observation hours near and after the Aqua overpass time.

In many cases the effects of clouds and changes in thermal contrast were seen to manifest concomitantly making it difficult to separate and properly quantify the exact contribution of each term to the reduction of the commission errors observed.

4.4. Reducing commission errors

From the results presented above it becomes clear that one of the major complications involved with the application of contextual fire detection methods over tropical forest regions is the effect of contrasting warm and bright surfaces surrounded by forest cover generating false detections. The parameters available with the MOD14 product metadata show significant overlap between true and false detections (Fig. 10), which eliminates the potential for successful post-processing of false detections using any of the available fire pixel information.

Another approach to resolve the commission errors affecting the two data sets is the use of temporal metrics to complement the spatial analysis provided by the contextual method. Change detection methods based on the application of temporal metrics to assess sudden variations in the pixel signature of moderate and coarse resolution sensors are growing in importance as satellite data sets with improved navigation quality become available (Calle et al., 2006; Koltunov & Ustin, 2007; Schaaf et al., 2002).

We selected over 100 detections from each of our MODIS and GOES validation data sets including true and false detections. Brightness temperatures (BT) were derived from the mid-infrared channels 21 and 22 of MODIS and channel 2 of GOES using MOD02 and GVAR Man computer Interactive Data Access System (McIDAS) AREA file data, respectively. The BT data were used to construct 30-day profiles from which the mean and standard deviation were extracted for each pixel. Fig. 11a and b shows a plot of the BT temporal profiles for two pixels fixed in space representing different cases of true and false detections in the MODIS and GOES data, respectively. The plots describe two important aspects of the data. First, MODIS shows a greater variability of the BT values compared to GOES, likely a function of variable imaging geometry. Despite its lower navigation quality, the GOES brightness temperatures show less variation over time. Second, since MODIS pixels are smaller compared to GOES, fires naturally occupy larger fractions of them, resulting in a greater departure from the mean value observed for the 30-day period analyzed. As a result, the potential limitations caused by a variable pixel size could be balanced by a high sensitivity to the presence of active fires within the pixel footprint, rendering this kind of application useful to separate false detections from true detections. On average, true detections departed by more than 4 standard deviations from the 30 day mean BT values, whereas for false detections the departure was limited to about 2 standard deviations. These results were equally valid for MODIS and GOES.

The graphs in Fig. 11 did not receive any rigorous treatment to reduce spurious oscillations in the derived BT values. Appropriate techniques could, however, be used for instance to model the daily variation of the MODIS BT data. In addition, the BT profiles in Fig. 11 benefit from the favorable conditions observed in Amazonia where stable surface temperature conditions prevail throughout most of the year (da Rocha et al., 2004). Nevertheless, the commission errors described above appear to be mainly associated with land use regimes marked by large deforestation rates typical of the tropical forest regions. In these regions, similar surface conditions should be expected.

5. Conclusions

In this study we presented a comprehensive validation analysis of the MOD14 and WFABBA fire detection products which are based on the MODIS and GOES data, respectively. We focused our analyses on the Brazilian part of Amazonia where vegetation fires are extensively used for tropical forest conversion and for maintenance of previously-deforested areas.

The two products tested utilize conceptually similar algorithms based on the use of contextual tests to detect pixels with active fires. However, these algorithms are applied to images of markedly different spatial and spectral resolutions. The resulting detection performance estimates obtained through the validation analysis indicated that an approximate factor of 4 separates the detection curves of MOD14 and WFABBA products, a relatively small difference compared to the 16× factor between their nominal spatial resolutions.

Although MODIS and GOES showed relatively high overall omission errors, their interpretation should be oriented by the type of application pursued. In this case, fire data users interested in larger biomass burning events may find both MODIS and GOES to have reasonably high rates of successful detections as is evidenced by the sharp decrease in omission errors especially near the low end of fire clusters described in Fig. 5.

The background conditions associated with active deforestation regions in Amazonia had a major effect on the false detections produced with both products. False detections can span multiple days provided that the burning scars remain evident and similar thermal conditions are preserved between adjacent areas. The reduction in commission error rates observed towards the afternoon hours has important consequences for the derivation of the fire diurnal cycle using contextual algorithms. In this case, an enhanced contrast between morning and afternoon hours should be noticed if all potential false detections are removed from the data.

Removal of false detections based on the metrics which are routinely produced by the contextual algorithms proved difficult. Alternatively, we successfully tested the application of temporal metrics of brightness temperature to isolate false detections in our data set. The use of a hybrid fire detection algorithm which implements change detection methods in addition to the contextual tests appears promising especially over tropical regions. In these areas, stable surface thermal conditions might facilitate the extraction of temporal metrics which could be used to separate false detections or increase our confidence about the true ones. However, we recognize that this is a topic for further

investigation necessitating careful consideration of all aspects involved.

The results described above are valid for open sky fires typical of forest conversion and agricultural maintenance in Amazonia, but do not apply to cases of understory burning. Although a few sub-canopy fires could be visually confirmed in our validation data, proper identification of those events via automated detection was difficult even at the 30 m resolution level. Consequently, detection of active understory fires using MODIS or GOES data appears to be significantly difficult using standard mid-infrared detection algorithms.

Another limitation of our analyses involves the conversion of 30 m active fire pixels statistics derived from ASTER and ETM+ into fire area and temperature estimates. Although theoretical assessment of ASTER channel 8 saturation was attempted relating minimum fire area and temperature (Giglio et al., in press), a more complete characterization of fire properties is still under investigation. Advancement in this area is limited primarily by inadequate specifications of existing orbital sensors.

This study extends a series of validation analyses applied to the MODIS *Thermal Anomalies* product and is the first one of its kind applied to the GOES WFABBA product. Our results corroborate previous findings and include new aspects involving the performance of the MODIS and GOES fire detection algorithms which can help the fire data user community optimize their use of these products.

Lessons learned from the validation of MODIS and GOES imager will be used to develop validation procedures for the fire products from new generation of US polar orbiter (NPOESS Visible Infrared Imager Radiometer Suite VIIRS) and geostationary (GOES-R Advance Baseline Imager — ABI) platforms. Of particular importance is the development of a multi-platform validation system and the quantification of validation errors stemming from the use of non-simultaneous space-based or airborne reference data. In addition, the better understanding of the detection envelopes of MODIS and GOES imager derived from this study can be used to assess the expected performance of the higher resolution VIIRS and ABI fire products.

Acknowledgments

A heartfelt thanks is dedicated to the late Alexandre Santos who so cheerfully helped with the implementation of the thermal couple data collection during three separate field campaigns. We thank Luiz Augusto Machado, Alberto Setzer, Juan Ceballos, Luis Maurano and the Environmental Satellite Division (DSA/INPE) in Cachoeira Paulista, Brazil for contributing with valuable ETM+ data for this study. We thank SIPAM and the entire flight crew and support personnel from the Brazilian Air Force's 2º/6º Flight Squadron in Anápolis, Brazil for operating the AHS sensor during the field campaign in Roraima 2003. We are thankful for the formidable support provided by the Municipal Fire Brigades in Roraima and Pará states. Also of great value were Geraldo Lucatelli, João Raposo Pereira, João Alexandre Perotto, Joaquim Toledo, Antonio Cattaneo and many others from the PROACO and PREVFOGO fire management programs at the IBAMA offices in Brasília, Boa Vista, Santarém and Marabá, who helped during many stages of the field work implemented. This study was in part funded by the Large Scale Biosphere-Atmosphere Experiment in Amazonia (LBA-ECO Phases II and III). The first author is a NASA Earth and Space Science Fellowship awardee.

Appendix A. ETM+ active fire mask

In order to improve our sampling capacity of the GOES data, a new 30 m fire mask product was created using Landsat 7 Enhanced Thematic Mapper Plus (ETM+) imagery. Due to similarities in spectral and spatial resolution between the ASTER and ETM+ data, the new ETM+ fire mask product builds on the Giglio et al. (in press) algorithm used to produce the ASTER product. Denoting the ETM+ channel 4 and 7 top-of-atmosphere reflectance as ρ_4 and ρ_7, respectively, unambiguous fire pixels are classified using the criteria:

$$R_{74} = \frac{\rho_7}{\rho_4} > 2.5$$
$$D_{74} = \rho_7 - \rho_4 > 0.3$$

Next, candidate pixels are selected based on the following tests:

$$R_{74} > 1.8$$
$$D_{74} > 0.17 \cdot$$

We apply a fixed 61×61 window centered on the candidate pixel to calculate the background statistics which will be used for the contextual part of the detection code. The mean and standard deviation are calculated for the reflectance ratio ($\overline{R_{74}}$ and σ_{R74}, respectively) and for channel 7 reflectance ($\overline{\rho_7}$ and $\sigma_{\rho 7}$, respectively). Unambiguous fire pixels and water pixels (pixels for which $\rho_7 < 0.04$) are excluded from the computation. Candidate pixels which satisfy the following conditions are classified as fires:

$$R_{74} > \overline{R}_{74} + \mathrm{Max}\left(3\sigma_{R74}, 0.8\right)$$
$$\rho_7 > \overline{\rho_7} + \mathrm{Max}\left(3\sigma_{\rho 7}, 0.08\right)$$

where the Max indicates that the maximum value is to be used. The numerical constants appearing in the tests were empirically derived for the scenes used in this study, and the resulting fire masks were visually inspected for consistency.

References

Agresti, A. (1990). *Categorical data analysis*.: John Wiley and Sons 558 pp.

Calle, A., Casanova, J. L., & Romo, A. (2006). Fire detection and monitoring using MSG Spinning Enhanced Visible and Infrared Imager (SEVIRI) data. *Journal of Geophysical Research*, *111*, G04S06. doi:10.1029/2005JG000116

Cochrane, M., Alencar, A., Schulze, M. D., Souza, C. M., Jr., Nepstad, D. C., Lefebvre, P., et al. (1999). Positive feedbacks in the fire dynamic of closed canopy tropical forests. *Science*, *284*, 1832−1835.

Comision Nacional de Actividades Espaciales (CONAE), Geston de Emergencias, Argentina, URL: http://www.conae.gov.ar/WEB_Emergencias/Links de la Izquierda/Incendios/incendios.html, last visited: 2007, 23 November.

Centro de Previsão do Tempo e Estudos Climáticos (CPTEC) (2007, November 23). *Vegetation fire monitoring*.Brazil: Instituto Nacional de Pesquisas Espaciais URL: http://www.cptec.inpe.br/queimadas, last visited.

Csiszar, I., Denis, L., Giglio, L., Justice, C. O., & Hewson, J. (2005). Global fire distribution from MODIS. *International Journal of Wildland Fire*, *14*, 117−130.

Csiszar, I., Morisette, J. T., & Giglio, L. (2006). Validation of active fire detection from moderate-resolution satellite sensors: the MODIS example in Northern Eurasia. *IEEE Transactions on Geoscience and Remote Sensing*, *44*(7), 1757−1764.

Csiszar, I., & Schroeder, W. (2007). Fire observations from ETM+ and ASTER imagery and implications for active fire product validation from coarse resolution sensors. *Proceedings of the 6th international workshop of the EARSeL special interest group on forest fires, 27–29 September 2007 Thessaloniki, Greece*. Luxembourg: JRC Scientific and Technical Reports, Office for Official Publications of the European Communities.

da Rocha, H. R., Goulden, M. L., Miller, S. D., Menton, M. C., Pinto, L. D. V. O., de Freitas, H. C., et al. (2004). Seasonality of water and heat fluxes over a tropical forest in eastern Amazonia. *Ecological Applications*, *14*(4), S22−S32.

Direccion de Manejo de Recusos Naturales (DIMARENA), Gobierno Departamental Prefectura Santa Cruz, Bolivia, URL: http://servicios.santacruz.gov.bo/forestal/index.php?option=com_mamboezine&Itemid=36, last visited:2007, 23 November.

Dwyer, E., Pinnock, S., Grégoire, J. -M., & Pereira, J. M. C. (2000). Global spatial and temporal distribution of vegetation fires as determined from satellite observations. *International Journal of Remote Sensing*, *21*, 1289−1302.

Freitas, S. R., Longo, K. M., Silva Dias, M. A. F., Silva Dias, P. L., Chatfield, R., Prins, E., et al. (2005). Monitoring the transport of biomass burning emissions in South America. *Environmental Fluid Mechanics*, *5*, 135−167.

Giglio, L. (2007). Characterization of the tropical diurnal fire cycle using VIRS and MODIS observations. *Remote Sensing of Environment*, *108*, 407−421.

Giglio, L., Csiszar, I., & Justice, C. O. (2006). Global distribution and seasonality of active fires as observed with the Terra and Aqua Moderate Resolution Imaging Spectroradiometer (MODIS) sensors. *Journal of Geophysical Research*, *111*, G02016. doi:10.1029/2005JG000142

Giglio, L., Csiszar, I., Restas, A., Morisette, J. T., Schroeder, W., Morton, D., et al. (in press). Active fire detection and characterization with the Advanced Spaceborne Thermal Emission and Reflection Radiometer (ASTER). *Remote Sensing of Environment*.

Giglio, L., Descloiters, J., Justice, C. O., & Kaufman, Y. (2003). An enhanced contextual fire detection algorithm for MODIS. *Remote Sensing of Environment*, *87*, 273−282.

Govaerts, Y. M., Wooster, M., Lattanzio, A., & Roberts, G. (2007). *MSG/SEVIRI fire thermal anomaly (FTA) characterization ATBD, EUMETSAT, Report EUM/MET/SPE/06/0398* (pp. 32).

Goward, S. N., Masek, J. G., Williams, D. L., Irons, J. R., & Thompson, R. J. (2001). The Landsat 7 mission terrestrial research and applications for the 21st century. *Remote Sensing of Environment*, *78*, 3−12.

Hansen, M. C., DeFries, R. S., Townshend, J. R. G., Sohlberg, R., Dimiceli, C., & Carroll, M. (2002). Towards an operational MODIS continuous fields of percent tree cover algorithm: examples using AVHRR and MODIS data. *Remote Sensing of Environment*, *83*, 303−319.

Kaufman, Y. J., Hobbs, P. V., Kirchhoff, V. W., Artaxo, P., Remer, L. A., Holben, B. N., et al. (1998). Smoke, Clouds, and Radiation-Brazil (SCAR-B) experiment. *Journal of Geophysical Research*, *103*, 31,783−31,808.

Korontzi, S., Roy, D. P., Justice, C. O., & Ward, D. E. (2004). Modelling and sensitivity analysis of fire emissions in southern Africa during SAFARI 2000. *Remote Sensing of Environment*, *92*, 376−396.

Koltunov, A., & Ustin, S. L. (2007). Early fire detection using non-linear multitemporal prediction of thermal imagery. *Remote Sensing of Environment*, *110*, 18−28.

Menzel, W. P., & Prins, E. M. (1996). Monitoring biomass burning with the new generation of geostationary satellites. In J. S. Levine (Ed.), *Biomass burning and global change* (pp. 56−64). Cambridge, MA: The MIT Press.

Menzel, W. P., & Purdom, J. F. W. (1994). Introducing GOES-I: the first of a new generation of geostationary operational environmental satellites. *Bulletin of the American Meteorological Society*, *75*(5), 757−781.

Morisette, J. T., Giglio, L., Csiszar, I., Setzer, A., Schroeder, W., Morton, D., et al. (2005). Validation of MODIS active fire detection products derived from two algorithms. *Earth Interactions*, *9*(paper no. 9), 1−25.

Morisette, J. T., Giglio, L., Csiszar, I., & Justice, C. O. (2005). Validation of the MODIS active fire product over Southern Africa with ASTER data. *International Journal of Remote Sensing*, *26*(19), 4239−4264.

Nepstad, D. C., Veríssimo, A., Alencar, A., Nobre, C., Lima, E., Lefebvre, P., et al. (1999). Large-scale impoverishment of Amazonian forests by logging and fire. *Nature*, *398*, 505−508.

Prins, E. M., Feltz, J. M., Menzel, W. P., & Ward, D. E. (1998). An overview of GOES-8 diurnalfire and smoke results for SCAR-B and 1995 fire season in South America. *Journal of Geophysical Research*, *103*(D24), 31.821−31.835.

Prins, E. M., & Menzel, W. P. (1992). Geostationary satellite detection of biomass burning in South America. *International Journal of Remote Sensing*, *13*, 2783−2799.

Prins, E. M., & Menzel, W. P. (1994). Trends in South American biomass burning detected with the GOES VAS from 1983–1991. *Journal of Geophysical Research*, *99*(D8), 16719−16735.

Prins, E.M., Schmidt, C.C., Feltz, J.M., Reid, J.S., Wesphal, D.L., & Richardson, K. (2003). A two year analysis of fire activity in the Western Hemisphere as observed with the GOES Wildfire Automated Biomass Burning Algorithm. Preprints, 12th Conf. on Satellite Meteorology and Oceanography, Long Beach, CA, Amer. Meteor. Soc., CD-ROM, P2.28.

Schaaf, C. B., Gao, F., Strahler, A. H., Lucht, W., Li, X., Tsang, T., et al. (2002). First operational BRDF, albedo nadir reflectance products from MODIS. *Remote Sensing of Environment*, *83*, 135−148.

Schroeder, W., Morisette, J. T., Csiszar, I., Giglio, L., Morton, D., & Justice, C. (2005). Characterizing vegetation fire dynamics in Brazil through multisatellite data: common trends and practical issues. *Earth Interactions*, *9* Paper 13.

Schroeder, W., Csiszar, I., & Morisette, J. (2008). Quantifying the impact of cloud obscuration on remote sensing of active fires in the Brazilian Amazon. *Remote Sensing of Environment*, *112*, 456−470. doi:10.1016/j.rse.2007.05.004

Setzer, A. W., & Pereira, M. C. (1991). Amazonia biomass burnings in 1987 and an estimate of their tropospheric emissions. *Ambio*, *20*(1), 19−22.

UW Madison Cooperative Institute for Meteorological Satellite Studies (CIMSS) Biomass Burning Monitoring Program, URL: http://cimss.ssec.wisc.edu/goes/burn/wfabba.html, last visited: 2007, 19 December.

Van der Werf, G. R., Randerson, J. T., Collatz, G. J., & Giglio, L. (2003). Carbon emissions from fires in tropical and subtropical ecosystems. *Global Change Biology*, *9*, 547−562.

Wolfe, R. E., Nishihama, M., Fleig, A. J., Kuyper, J. A., Roy, D. P., Storey, J. C., et al. (2002). Achieving sub-pixel geolocation accuracy in support of MODIS land science. *Remote Sensing of Environment*, *83*, 31−49.

Yamaguchi, Y., Kahle, A. B., Tsu, H., Kawakami, T., & Pinel, M. (1998). Overview of advanced spaceborne thermal emission and reflection radiometer (ASTER). *IEEE Transactions on Geoscience and Remote Sensing*, *36*, 1062−1071.